

Intricate Magnetic Interactions and Topological Hall Effect Observed in Itinerant Room-temperature Layered Ferromagnet $\text{Cr}_{0.83}\text{Te}$

Shubham Purwar, Susmita Changdar, Susanta Ghosh, Tushar Kanti Bhowmik and Setti Thirupathaiah*

S. N. Bose National Centre for Basic Sciences, Salt Lake, JD Block, Sector III, Bidhannagar, Kolkata, 700106, West Bengal, India

ARTICLE INFO

Keywords:

2D Magnetism
Magnetocaloric effect
Magneto-entropy scaling
Topological Hall effect
Magnetic anisotropy

ABSTRACT

We report the magnetic, electrical, and magnetotransport (Hall effect) properties of the hexagonal itinerant ferromagnet $\text{Cr}_{0.83}\text{Te}$. Further, a comprehensive study of the magneto-entropy scaling behavior has been done around the Curie temperature of $T_C \approx 338$ K. A maximum entropy change ($-\Delta S_m^{\max}$) of $2.77 \text{ J/kg} - \text{K}$ and relative cooling power (RCP) of 88.29 J/kg near the T_C have been achieved under an applied magnetic field of 5 Tesla. The critical exponents, $\beta = 0.4739(4)$, $\gamma = 1.2812(3)$, and $\delta = 3.7037(5)$, have been extracted using the magneto-entropy scaling analysis. The obtained critical exponents indicate the presence of intricate magnetic interactions in $\text{Cr}_{0.83}\text{Te}$. On the other hand, the magnetotransport study reveals a topological Hall effect attributed to the noncoplanar spin structure coexisting with a robust magnetocrystalline anisotropy. Further, we observe that the extrinsic skew-scattering mechanism originated anomalous Hall effect. Our experimental findings of the anomalous and topological Hall effect properties in the presence of intriguing high-temperature itinerant ferromagnetism and magnetocaloric effect in $\text{Cr}_{0.83}\text{Te}$ can offer potential technological applications at room temperature.

1. Introduction

Investigation of the low dimensional magnetic materials with ferromagnetic ordering at room temperature and strong magnetocrystalline anisotropy [1, 2] has gained a lot of research interests in recent days due to their potential applications in magnetic refrigeration and spintronic devices [3–8]. Hence, the van der Waals (vdW) ferromagnets are of great research interest from the fundamental science and advanced technology point of view due to their peculiar two-dimensional (2D) magnetic properties [9–12] and strong magnetocrystalline anisotropy [13]. Usually, the Heisenberg-type ferromagnet does not exist with intrinsic long-range magnetic ordering at finite temperature in the 2D limit due to dominant thermal fluctuations [14]. Nevertheless, the single domain anisotropy or the exchange anisotropy can overcome the thermal fluctuation and allow the long-range magnetic ordering in 2D ferromagnets [15]. In this way, the 2D ferromagnetism has been found experimentally in many vdW materials such as $\text{Cr}_2\text{Ge}_2\text{Te}_6$ ($T_C \approx 61$ K) [16], $\text{Cr}_2\text{Si}_2\text{Te}_6$ ($T_C \approx 32$ K) [17, 18], Fe_3GeTe_2 ($T_C \approx 215$ K) [11, 19], and CrI_3 ($T_C \approx 45$ K) [15], but the long-range FM ordering temperature is far below the room temperature, limiting their usage in technological applications. Since a very few systems such as MnP ($T_C \approx 303$ K) show room temperature 2D ferromagnetism in the bulk phase [20], searching for new room-temperature layered FM materials coupled with large magnetocrystalline anisotropy is crucial for realizing potential technological applications.

Furthermore, the FM vdW materials possess another peculiar property such as the magnetocaloric effect (MCE).

The magnetocaloric effect (MCE) at room temperature in the FM vdW materials with maximum entropy change $-\Delta S_m^{\max}$ is of recent research interest due to their technological applications in the environmental friendly magnetic refrigerators [21]. There exists quite a few 2D FM systems showing significant $-\Delta S_m^{\max}$ such as $\text{Fe}_{3-x}\text{GeTe}_2$ ($1.1 \text{ J/kg} - \text{K}$ at 5 T) [22], Cr_5Te_8 ($1.6 \text{ J/kg} - \text{K}$ at 5 T) [23], $\text{Cr}_2\text{Si}_2\text{Te}_6$ ($5.05 \text{ J/kg} - \text{K}$ at 5 T), and $\text{Cr}_2\text{Ge}_2\text{Te}_6$ ($2.64 \text{ J/kg} - \text{K}$ at 5 T) [24].

Theoretical studies suggest that the layered Cr_xTe_y systems are the potential candidates to realize the much-anticipated room-temperature 2D ferromagnetism in bulk [25]. Since then, a variety of Cr_xTe_y compounds have been grown experimentally and studied for their peculiar 2D ferromagnetism, including CrTe [26], Cr_2Te_3 [27], Cr_3Te_4 [28], Cr_4Te_5 [29–31], and Cr_5Te_8 [32, 33]. Generally, Cr_xTe_y compounds possess alternating stacks of CrTe_2 layers intercalated by the Cr layers (excess) along the z -axis [34]. The intercalated Cr concentration plays an important role in the formation of these compounds' crystal structure, magnetic structure, and transport properties [35–38]. The topological Hall effect observed in Cr_xTe_y systems implies the presence of non-trivial spin texture such as skyrmions and bi-skyrmions [39, 40] or the noncoplanar magnetic structures [41–43].

On the other hand, though there exist a couple of studies on the hexagonal Cr_{1-x}Te type systems, discussing the magnetic, transport, and Hall effect properties [44, 45], no systematic study is available on the magnetocrystalline anisotropy (MCA) and magneto-entropy scaling analysis which offer a better understanding on the topological Hall effect and magnetic exchange interactions, respectively. Importantly, the magnetic exchange interactions are profoundly influenced by the MCA, manifesting the Heisenberg, XY,

*setti@bose.res.in (S. Thirupathaiah)

www.qmat.in (S. Thirupathaiah)

ORCID(s): 0000-0003-1258-0981 (S. Thirupathaiah)

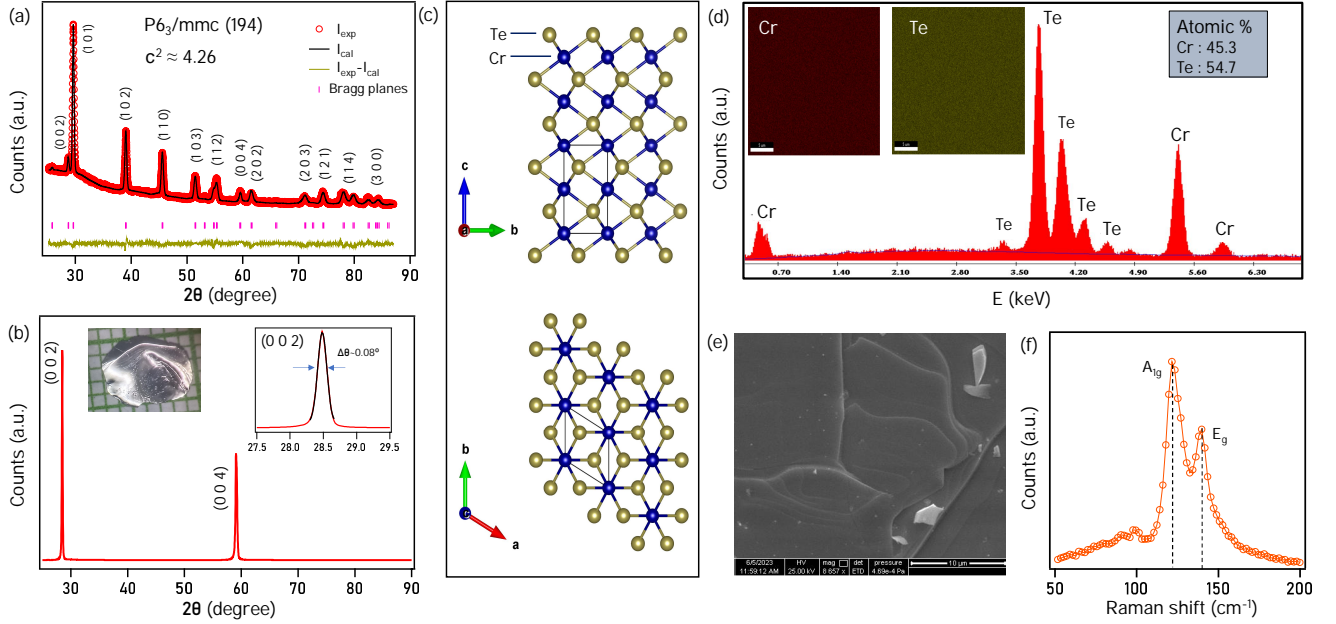


Figure 1: (a) Powder x-ray diffraction (XRD) of the crushed $\text{Cr}_{0.83}\text{Te}$ single crystals overlapped with Rietveld refinement. (b) XRD pattern of $\text{Cr}_{0.83}\text{Te}$ single crystal. The left inset of (b) shows the photographic image of a typical $\text{Cr}_{0.83}\text{Te}$ single crystal. The right inset of (b) shows the rocking curve of (0 0 2) Bragg's reflection with FWHM of 0.08° . (c) Schematics of the CrTe hexagonal crystal structure projected onto the bc -plane and ab -plane. (d) Energy dispersive X-ray spectroscopy (EDXS) spectra of $\text{Cr}_{0.83}\text{Te}$ single crystal. Top-insets of (d) show the elemental mapping of Cr and Te. (e) Scanning electron microscopy (SEM) image of $\text{Cr}_{0.83}\text{Te}$ single crystal. (f) Raman spectra of $\text{Cr}_{0.83}\text{Te}$ single crystal.

Ising, or complex magnets [46–48]. In addition, the strong MCA is crucial for engineering the non-coplanar spin-structure that leads to generating the skyrmion lattice [49, 50]. On the other hand, the magneto-entropy scaling analysis deduces the critical exponents, defining the strength and the type of magnetic interactions present in the system [23, 24, 51, 52].

Therefore, this study reports the anisotropic magnetic properties, anomalous and topological Hall effects, and magnetocaloric effect in the hexagonal $\text{Cr}_{0.83}\text{Te}$ single crystal. $\text{Cr}_{0.83}\text{Te}$ is an interesting system as it falls in between the van der Waals trigonal (vdW) CrTe_2 [53] and non-vdW hexagonal CrTe [54], despite all three being layered systems. As the intercalated Cr atoms play a vital role in shaping the magnetic and magnetotransport properties, $\text{Cr}_{0.83}\text{Te}$ could be a potential candidate to show the topological Hall effect (THE) originating from the noncoplanar spin structure of the intercalated Cr spins. Moreover, it is one of the few Cr_xTe_y type systems showing room temperature ferromagnetism, idle for room temperature technological applications such as magnetic storage devices [55], spin valves [56], magnetic tunnel junctions [56], and spin-transfer torque devices [57]. Although an earlier study on the similar composition of hexagonal $\text{Cr}_{0.833}\text{Te}$ (Cr_5Te_6) performed critical analysis but lacked details on the relation between the anisotropic magnetic properties and the topological Hall effect [58]. Another study performed magnetotransport measurements on a different crystal structure of monoclinic thin film $\text{Cr}_{0.833}\text{Te}$, yet lacks the discussion on the relation between MCA and

THE [41]. Therefore, this study aims to unravel the relation between the magnetocrystalline anisotropy, the topological Hall effect, and the magnetic exchange interactions in the hexagonal $\text{Cr}_{0.83}\text{Te}$. Further, the re-scaled magnetoentropy change, $-\Delta S_m(T, H)$, exhibits a remarkable convergence onto a universal curve, suggesting a second-order magnetic transition in this systems [59, 60]. Extracted critical exponents from the field-dependent magnetoentropy change highlight the interplay between the 3D-Ising and the meanfield-type exchange interactions.

2. Experimental details

High-quality single crystals of $\text{Cr}_{0.83}\text{Te}$ were grown using the chemical vapor transport (CVT) method with iodine as a transport agent. We thoroughly mixed Cr (99.99%, Alfa Aesar) and Te (99.99%, Alfa Aesar) powders in a 5 : 5 ratio, and a small quantity of iodine (3 mg/cc) was added to the powder mixture. The mixture was sealed in a quartz tube under argon gas and placed in a gradient two-zone horizontal tube furnace for about 15 days. One end of the tube was heated at 1000°C (source) and the other end was kept at 820°C (sink), following a previously established procedure [61]. The obtained single crystals were large, measuring up to $5 \times 5 \text{ mm}^2$, and looking shiny. A representative photographic image of a typical single crystal is shown in the inset of Fig. 1(b).

The crystal structure of as-grown $\text{Cr}_{0.83}\text{Te}$ single crystals was examined by the x-ray diffraction (XRD) technique using the Rigaku x-ray diffractometer (SmartLab, 9 kW)

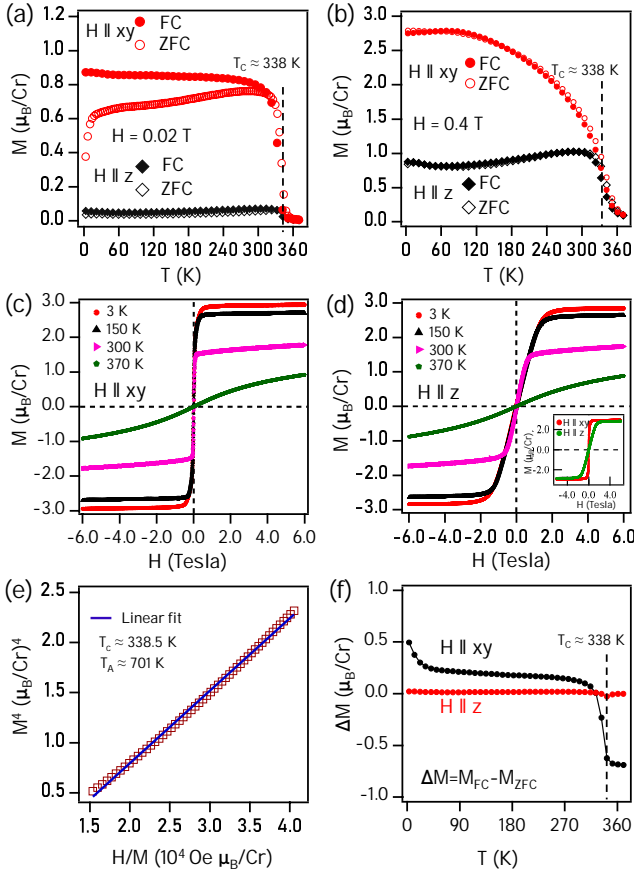


Figure 2: Temperature-dependent magnetization [$M(T)$] of $\text{Cr}_{0.83}\text{Te}$ taken in zero-field-cooled (ZFC) and field-cooled (FC) modes with magnetic fields $H = 0.02$ T (a) and 0.4 T (b) for $H \parallel xy$ and $H \parallel z$. Magnetization isotherms [$M(H)$] measured at various sample temperatures for (c) $H \parallel xy$ and (d) $H \parallel z$. (e) Plot of M^4 vs H/M . (f) Temperature-dependent ΔM ($M_{FC} - M_{ZFC}$) derived for $H \parallel xy$ and $H \parallel z$.

with Cu K_α radiation of wavelength of $\lambda = 1.5406$ Å. We employed scanning electron microscopy (SEM) and energy-dispersive X-ray spectroscopy (EDXS) techniques to explore surface morphology and elemental compositions. Magnetic and transport properties were studied by the physical property measurement system (9 Tesla-PPMS, DynaCool, Quantum Design). Electrical resistivity and Hall measurements were conducted using the conventional four-probe technique. To eliminate the influence of longitudinal magnetoresistance, caused mainly by the voltage probe misalignment, the Hall resistivity was determined as $\rho_{xy}(H) = [\rho_{xy}(+H) - \rho_{xy}(-H)]/2$. In addition, Raman spectra were captured using a micro-Raman spectrometer (LabRam HR Evolution HORIBA France SAS) equipped with a 532 nm laser.

3. Results and Discussion

3.1. Structural Properties

Figure 1(a) displays the XRD pattern of crushed $\text{Cr}_{0.83}\text{Te}$ single crystals taken at room temperature, confirming the hexagonal crystal structure with $P6_3/mmc$ space group. No

additional impurity phases were detected. Rietveld refinement, overlapped on the XRD data, yields lattice parameters $a = b = 3.9808(4)$ Å and $c = 6.2122(3)$ Å, which are very close to the previous reports on similar systems [44, 62]. Fig. 1(b) depicts the XRD pattern of $\text{Cr}_{0.83}\text{Te}$ single crystal, showing the intensity of $(00l)$ Bragg plane, suggesting that the crystal growth axis is along the c -axis. The rocking curve of (002) plane shown in the right-inset of Fig. 1(b) displays a single sharp peak with a full width at half maximum (FWHM) of $\Delta\theta = 0.08^\circ$, confirming the high quality of single crystals [63]. The crystal structure of $\text{Cr}_{0.83}\text{Te}$, as schematically presented in the top-panel of Fig. 1(c), reveals stacking of CrTe_2 layers along the c -axis arrangement without significant vdWs gap between two CrTe_2 layers. This arrangement differs from other Cr_xTe_y -based systems in which a significant vdW gap is present [42, 53]. From the crystal structure projected onto the ab -plane, as shown in the bottom-inset of Fig. 1(c), we can observe an intertwined honeycomb lattice consisting of Cr and Te atoms. Fig. 1(d) depicts the EDXS spectra, revealing the Cr:Te atomic ratio of 0.83:1, consistent with the chemical composition of $\text{Cr}_{0.83}\text{Te}$ obtained from the powder XRD refinement. The EDXS mappings shown in the insets of Fig. 1(d) confirm the uniform distribution of Cr and Te elements in the studied single crystal. The obtained sample composition of $\text{Cr}_{0.83}\text{Te}$ hints at the 17% of Cr vacancies. These vacancies seem critical in maintaining the NiAs-type hexagonal crystal structure [34, 44, 64]. Fig. 1(e) presents the SEM image of $\text{Cr}_{0.83}\text{Te}$ single crystal with terraces of the different layers, demonstrating the layered nature of the system. The Raman spectra of $\text{Cr}_{0.83}\text{Te}$ as shown in Fig. 1(f) unveil two prominent phonon peaks, positioned at approximately 123.5 cm^{-1} and 139.79 cm^{-1} . These peaks correspond to the distinct vibrational modes, the out-of-plane A_{1g} and the in-plane E_g , of the Cr_xTe_y system [64, 65].

3.2. Magnetic Properties

3.2.1. Magnetization Measurements

To explore the magnetic properties of $\text{Cr}_{0.83}\text{Te}$, we performed magnetization measurements as a function of temperature [$M(T)$] and field [$M(H)$]. The magnetic field was applied parallel to both the xy -plane [$H \parallel xy$] and the z -axis [$H \parallel z$]. Figs. 2(a) and 2(b) exhibit the in-plane ($H \parallel xy$) and out-of-plane ($H \parallel z$) $M(T)$ curves obtained under magnetic fields of 0.02 T and 0.4 T, respectively. As we can notice, the system undergoes a paramagnetic-to-ferromagnetic (PM-FM) transition at a Curie temperature (T_C) of approximately 338 K, very close to the previously reported value on a similar system [44]. The bifurcation in the $M(T)$ curves at T_C between ZFC and FC, as observed in Fig. 2(a), can be ascribed to the magnetic ordering, which is thermally irreversible at lower fields (0.02 T) due to canted magnetic moments [66, 67]. This interpretation is supported by the $M(T)$ data taken at 0.4 T of the applied field [see Fig. 2(b)], in which we can see the absence of bifurcation between ZFC and FC data at the T_C due to complete alignment of the canted moments along the field

direction. Further, at an applied field of 0.02 T, a sharp downturn in the ZFC $M(T)$ data is noticed at around 15 K, which disappears at 0.4 T, suggesting a possible spin-glass type transition below 15 K [68] at lower fields. Nevertheless, we notice significant magnetization anisotropy between in-plane and out-of-plane orientations at both applied fields.

Figs. 2(c) and 2(d) depict the magnetization isotherms, $M(H)$, measured at different temperatures for $H \parallel xy$ and $H \parallel z$ orientations, respectively. The $M(H)$ data suggest Cr_{0.83}Te to be a soft-ferromagnet with negligible coercivity. The magnetic anisotropy observed from the $M(T)$ data is further verified by the magnetization isotherms by plotting in-plane and out-of-plane $M(H)$ at 3 K, as shown in the inset of Fig. 2(d). The magnetic anisotropy observed in these systems plausibly stems from the non-coplanar magnetic structure resulting from the Cr vacancies [41, 42]. From Figs. 2(c) and 2(d), it is clear that Cr_{0.83}Te has an easy-axis parallel to the xy -plane. This observation is substantiated by the magnetization saturation occurring at an applied field of 0.5 T for $H \parallel xy$. In comparison, 1.9 T is needed for the same with $H \parallel z$ when measured at 3 K. Note here that an easy-axis of magnetization parallel to the z -axis was found from a similar system of Cr_{0.87}Te which has 4.6% of higher Cr compared to our studied Cr_{0.83}Te, again confirming that the magnetic structure is highly sensitive to the Cr concentration present in these systems [39, 69]. The saturation magnetization (M_s) for both in-plane and out-of-plane orientations is determined as 2.95 μ_B/Cr and 2.86 μ_B/Cr , respectively. This is notably smaller than the calculated ordered moment of Cr (3.4 μ_B/Cr) from the band structure calculations due to the itinerant nature of the Cr- d electrons [34, 70].

Next, to estimate the degree of itinerant ferromagnetism in Cr_{0.83}Te, we employed Takahashi's self-consistent renormalization (SCR) theory around T_C [71]. According to the SCR theory, the magnetization M and the magnetic field H at T_C are related by,

$$M^4 = \frac{1}{4.671} \left[\frac{T_C^2}{T_A^3} \right] \left(\frac{H}{M} \right) \quad (1)$$

Here, T_A denotes the dispersion of the spin fluctuation spectrum in the wave-vector space. Fig. 2(e) shows the M^4 vs. H/M for $H \parallel xy$, fitted nicely by the linear Eq. 1. This linear relationship is generally observed in itinerant ferromagnetic systems like LaCo₂P₂ ($T_C/T_0 \approx 0.14$) [72], Fe₄GeTe₂ ($T_C/T_0 \approx 0.16$) [73], SmCoAsO ($T_C/T_0 \approx 0.12$) [74], and Cr₄Te₅ ($T_C/T_0 \approx 0.063$) [30]. The fit yields a slope of $7.2168 \times 10^{-5} [\mu_B/\text{Cr}]^5/\text{Oe}$. Using the slope and T_C values, we estimate T_A to be approximately 701 K for $H \parallel xy$. As per the SCR theory, the T_C can be described by,

$$T_C = (60c)^{-3/4} M_{sp}^{3/2} T_A^{3/4} T_0^{1/4} \quad (2)$$

Here, $c = 0.3353$, M_{sp} represents the spontaneous magnetization, and T_0 denotes the energy width of the dynamical

spin fluctuation spectrum. Using the values of T_C , M_{sp} , and T_A , we deduce the characteristic temperature $T_0 = 4963$ K for Cr_{0.83}Te. Further, the SCR spin fluctuation theory suggests that the ratio T_C/T_0 defines the degree of itineracy in the ferromagnets. Such as, the spin moments are localized for $T_C/T_0 \approx 1$ and delocalized for $T_C/T_0 \ll 1$ [75]. In Cr_{0.83}Te single crystals, we estimate $T_C/T_0 \approx 0.07 (\ll 1)$, confirming the itinerant ferromagnetic behavior.

Fig. 2(f) depicts $\Delta M (M_{FC} - M_{ZFC})$ plotted as a function of temperature for both $H \parallel z$ and $H \parallel xy$. From Fig. 2(f) it is evident that the out-of-plane magnetization does not change much between ZFC and FC modes, while the ΔM of in-plane magnetization is very sensitive at around T_C . More importantly, ΔM rapidly increases with decreasing temperature below 40 K. This kind of magnetic behavior could stem from multiple factors, including the inherent magnetic anisotropy of these systems [32, 44] or the noncoplanar magnetic structure resulting from the Cr vacancies [41, 42].

3.2.2. Magnetocrystalline Anisotropy

With the help of magnetization isotherms [$M(H)$] as shown in the Figs. 3(a) and 3(b), we studied the magnetocrystalline anisotropy (MCA) energy density (K_u) using the expression [40],

$$K_u = \mu_0 \int_0^{M_s} [H_{xy}(M) - H_z(M)] dM \quad (3)$$

Here M_s denotes the saturation magnetization. H_{xy} and H_z represent the fields applied along xy and z directions, respectively. Fig. 3(c) depicts the temperature-dependent K_u derived from the experimental data. We find $K_u = 78.11$ kJ/m³ at $T = 310$ K, gradually decreasing with increasing temperature and reaching 23.73 kJ/m³ at T_C (338 K). On the other hand, the estimated $K_u \approx 390$ kJ/m³ at 40 K [see Fig. 6(d)] is much larger than the K_u values reported on many 2D magnetic systems such as CrBr₃ [76], Cr₂Ge₂Te₆ [24], and Cr₂Si₂Te₆ [24] and comparable to the K_u values of CrI₃ [76] and Fe₄GeTe₂ [73, 77]. Though Fe₃GeTe₂ shows a large magnetocrystalline anisotropy of 1460 kJ/m³ at 2 K [78], its Curie temperature is much below the room temperature ($T_C = 220$ K) [78]. Thus, Cr_{0.83}Te having a large K_u value of ≈ 390 kJ/m³ with a Curie temperature of 338 K seems to be a promising candidate from the technological applications point of view. See Table 1 for a list of 2D materials and their respective magnetocrystalline anisotropy energies (K_u).

Since the magnetic anisotropy expectation value $\langle K^n \rangle$ is directly proportional to $M_s^{n(n+1)/2}$, as per the classical theory of magnetism [79, 80], we plotted $[\frac{M_s(T)}{M_s(310)}]^{n(n+1)/2}$ for $n = 1, 2$, and 4. Here, $n = 1$ represents intrinsic anisotropy, $n = 2$ represents uniaxial anisotropy, and $n = 4$ represents cubic anisotropy, giving rise to the exponents 1, 3, and 10, respectively. In Fig. 3(d), we plotted $[M_s(T)/M_s(310)]$, $[M_s(T)/M_s(310)]^3$, and $[M_s(T)/M_s(310)]^{10}$ ratios as a function of temperature. Most importantly, in Fig. 3(d), the overlapped $K_u(T)$ of Fig. 3(c) matches very well with

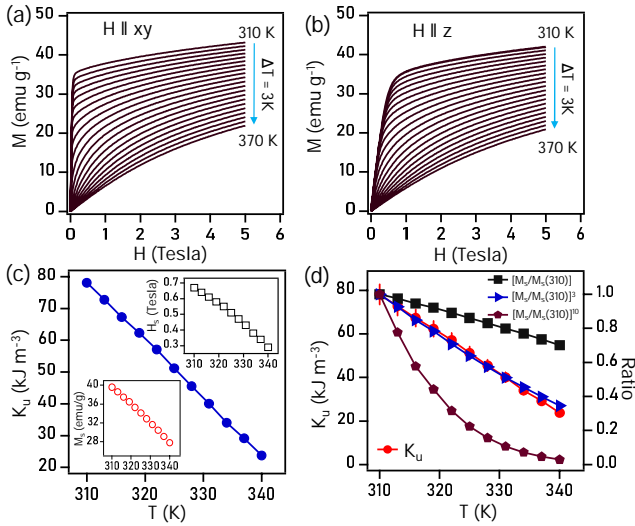


Figure 3: Magnetization isotherms measured around T_C for (a) $H \parallel xy$ and (b) $H \parallel z$. (c) Temperature-dependent in-plane magnetocrystalline anisotropy energy density K_u . The bottom inset in (c) presents saturation magnetization (M_s) and the top inset shows saturation magnetic field (H_s) estimated below T_C . (d) Ratios of $[M_s/M_s(310 K)]^{n(n+1)/2}$ (right-axis) overlaid with magnetocrystalline anisotropy (left-axis) for $n = 1, 2$, and 4 .

Table 1

Magnetocrystalline anisotropy energies (K_u) of different layered materials.

Composition	$\approx K_u$ (in kJ/m ³)	Ref.
Cr _{0.83} Te	390	This work
Cr _{0.87} Te	270	[44]
Cr _{0.69} Te	165	[42]
Cr _{0.625} Te	94	[23]
Cr _{0.6} Te	174	[43]
CrBr ₃	86	[76]
CrI ₃	300	[76]
Cr ₂ Ge ₂ Te ₆	20	[24]
Cr ₂ Si ₂ Te ₆	65	[24]
Fe ₄ GeTe ₂	250	[77]
Fe ₃ GeTe ₂	1460	[78]

$[M_s(T)/M_s(310 K)]^3$ ratio, confirming the dominant uniaxial anisotropy in this system that is strongly temperature dependent. The temperature-dependent K_u originates from the fluctuating local spin clusters activated from the thermal energy [79, 80].

3.2.3. Magnetocaloric Effect

To investigate the magnetocaloric effect (MCE), we analyzed the field-dependent isotherms $M(H)$ acquired at different temperatures [see Figs. 3(a) and 3(b)] in the vicinity of T_C for both $H \parallel xy$ and $H \parallel z$ orientations. The

magnetocaloric effect is an intrinsic property of a ferromagnetic system, resulting from adiabatic heating or cooling under external magnetic fields [81]. This effect leads to the generation of magnetic entropy change $\Delta S_m(T, H)$, which can be quantified using the formula,

$$\Delta S_m(T, H) = \int_0^H \left(\frac{\partial S}{\partial H} \right)_T dH = \int_0^H \left(\frac{\partial M}{\partial T} \right)_H dH \quad (4)$$

where $(\frac{\partial S}{\partial H})_T = (\frac{\partial M}{\partial T})_H$ based on Maxwell's relation. For the magnetization data acquired at smaller discrete field and temperature intervals, the magnetic entropy change $\Delta S_m(T, H)$ can be expressed as

$$\Delta S_m(T, H) = \frac{\int_0^H M(T_{i+1}, H) dH - \int_0^H M(T_i, H) dH}{T_{i+1} - T_i} \quad (5)$$

Figs. 4(a) and 4(b) show $-\Delta S_m(T, H)$ plotted as a function temperature under various magnetic fields up to 5 T taken with a step size of 1 T for both $H \parallel xy$ and $H \parallel z$ orientations, respectively. All $-\Delta S_m(T, H)$ curves show a maximum change in entropy with a broad peak at around T_C as can be seen from Figs. 4(a) and 4(b). Further, we observe that the value of $-\Delta S_m^{max}(T, H)$ increase monotonically with field for $H \parallel xy$ [see Fig. 4(c)]. Under an applied field of 5 T, the maximum of $-\Delta S_m(T, H)$ is about 2.78 J kg⁻¹ K⁻¹ for $H \parallel xy$ and is about 2.58 J kg⁻¹ K⁻¹ for $H \parallel z$. These $-\Delta S_m(T, H)$ values taken at 5 T are comparable to the other 2D ferromagnetic systems such as Cr₂Ge₂Te₆ (2.64 J kg⁻¹ K⁻¹) [24] and Cr₅Te₈ (2.38 J kg⁻¹ K⁻¹) [23], larger than the values of Fe_{3-x}GeTe₂ (1.14 J kg⁻¹ K⁻¹) [83] and CrI₃ (1.56 J kg⁻¹ K⁻¹) [84], and smaller than the values of CrBr₃ (7.2 J kg⁻¹ K⁻¹) [85] and Cr₂Si₂Te₆ (5.05 J kg⁻¹ K⁻¹) [24].

To estimate the relative cooling power (RCP) as shown in Fig. 4(c), we employed the relation $RCP = -\Delta S_m^{max} \times \delta T_{FWHM}$, where $-\Delta S_m^{max}$ is the maximum entropy change near T_C and δT_{FWHM} is the full width at half maximum of the peak [86]. The calculated RCP in Cr_{0.83}Te is 88.29 J kg⁻¹ at around T_C with an applied field of 5 T parallel to the xy -plane. The RCP value of Cr_{0.83}Te obtained in this study is comparable to the RCP value obtained in the other 2D systems such as Cr₂Ge₂Te₆ (87 J kg⁻¹) [24], but smaller than the values obtained from Cr₅Te₈ (131.2 J kg⁻¹) [23], CrI₃ (122.6 J kg⁻¹) [84], Cr₂Si₂Te₆ (114 J kg⁻¹) [24], Fe_{3-x}GeTe₂ (113 J kg⁻¹) [83], and CrBr₃ (191.5 J kg⁻¹) [85].

In addition, both $-\Delta S_m^{max}$ and RCP are related by the power law of magnetic field as given below [86, 87],

$$-\Delta S_m^{max} = aH^p \quad (6)$$

$$RCP = bH^q \quad (7)$$

where p and q are the exponents. At $T = T_C$, they can be written as

$$p = 1 + \frac{\beta - 1}{\beta + \gamma} \quad (8)$$

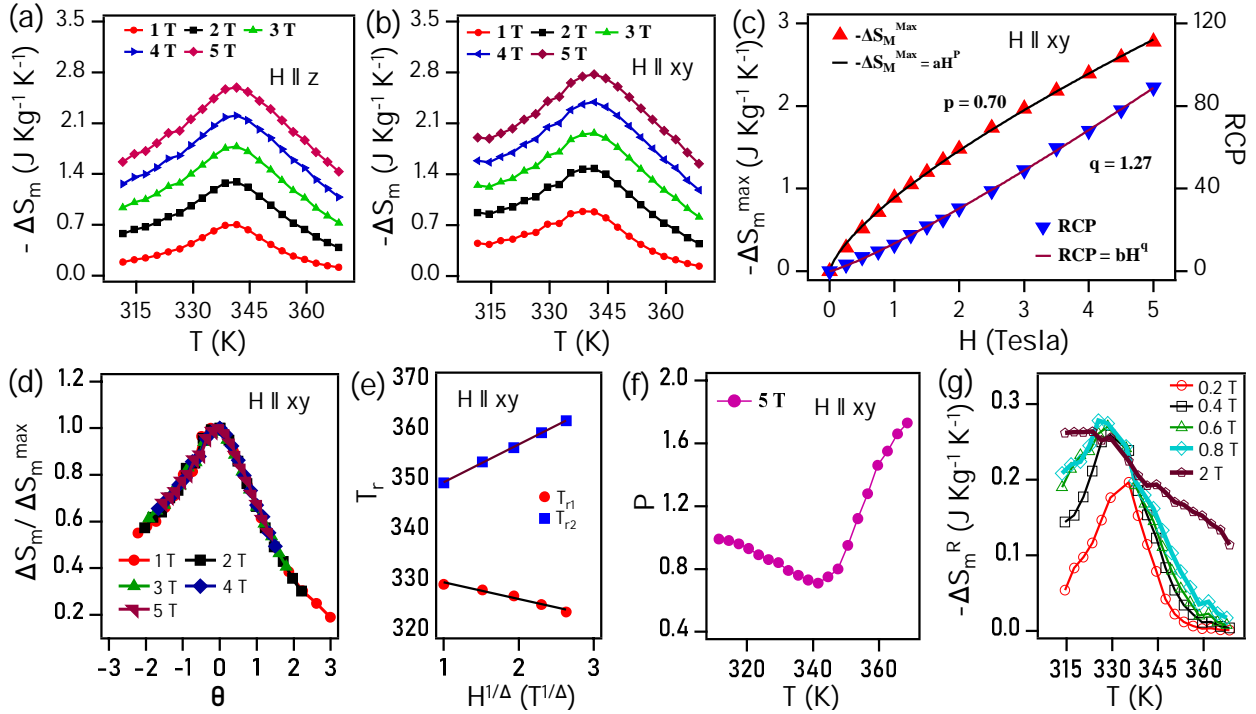


Figure 4: Magnetic entropy change $-\Delta S_m$ plotted as a function of temperature at different magnetic fields for (a) $H \parallel z$ and (b) $H \parallel xy$. (c) Field-dependent maximum magnetic entropy change ($-\Delta S_m^{\max}$) (left axis) and relative cooling power (RCP) (right axis). (d) Normalized magnetic entropy change as a function of rescaled temperature θ for various applied fields. (e) T_r vs $H^{1/\Delta}$. (f) Exponent p plotted as a function of temperature. (g) Rotational magnetic entropy change ($-\Delta S_m^R$) plotted as a function of temperature.

Table 2

Critical exponents of Cr_{0.83}Te single crystal compared with several theoretical models (MEC = Magnetic Entropy Change).

Composition	Technique	β	γ	δ	p	q	Ref.
Cr _{0.83} Te	MEC	0.4739(4)	1.2812(3)	3.7037(5)	0.70	1.27	This work
Landau mean field	Theory	0.5	1	3	0.667	1.333	[82]
3D Heisenberg	Theory	0.365	1.386	4.80	0.637	1.208	[46]
3D Ising	Theory	0.325	1.241	4.82	0.569	1.207	[46]

$$q = 1 + \frac{1}{\delta} \quad (9)$$

Where β , γ , and δ are critical exponents, which can be found using alternative theoretical models such as isothermal analysis, these exponents obtained from the magnetic entropy analysis, however, are more dependable without the use of initial exponents. In addition, the exponent δ has been calculated using the Widom scaling relation, $\delta = 1 + (\gamma/\beta)$ [88]. The fit of $-\Delta S_m^{\max}$ by the Eq. 6 yields $p = 0.70$. Similarly, the field dependence of RCP is fitted by Eq. 7, yielding $q = 1.27$. Based on Eq. 8 and Eq. 9, the derived critical exponents are $\beta = 0.4739(4)$, $\gamma = 1.2812(3)$, and $\delta = 3.7037(5)$. Note that no single conventional universality class can describe the derived critical exponents. The

critical exponents suggest a crossover between the mean-field model ($\beta = 0.5$) and the 3D-Ising model ($\gamma = 1.241$). Thus, our study indicates complex magnetic interactions in the Cr_{0.83}Te system.

Next, we performed the scaling analysis of MCE following the procedure given by Franco *et al.* [87, 89]. The scaling analysis of $-\Delta S_m(T, H)$ is constructed by normalizing the $-\Delta S_m(T, H)$ curves with respect to the maximum of $-\Delta S_m^{\max}$ [$\frac{\Delta S_m(T, H)}{\Delta S_m^{\max}}$]. The reduced temperature (θ_{\mp}) is defined by choosing two reference temperatures ($T_{r1} \leq T_C$ and $T_{r2} > T_C$), satisfying the condition, $\frac{\Delta S_m(T_{r1} < T_C)}{\Delta S_m^{\max}} = \frac{\Delta S_m(T_{r2} > T_C)}{\Delta S_m^{\max}} = h$. Here, h is a scaling constant with values within the $0 < h < 1$ range. Then, the rescaled temperature θ_{\mp} can be written as

$$\theta_{-} = (T_C - T)/(T_{r1} - T_C), T \leq T_C \quad (10)$$

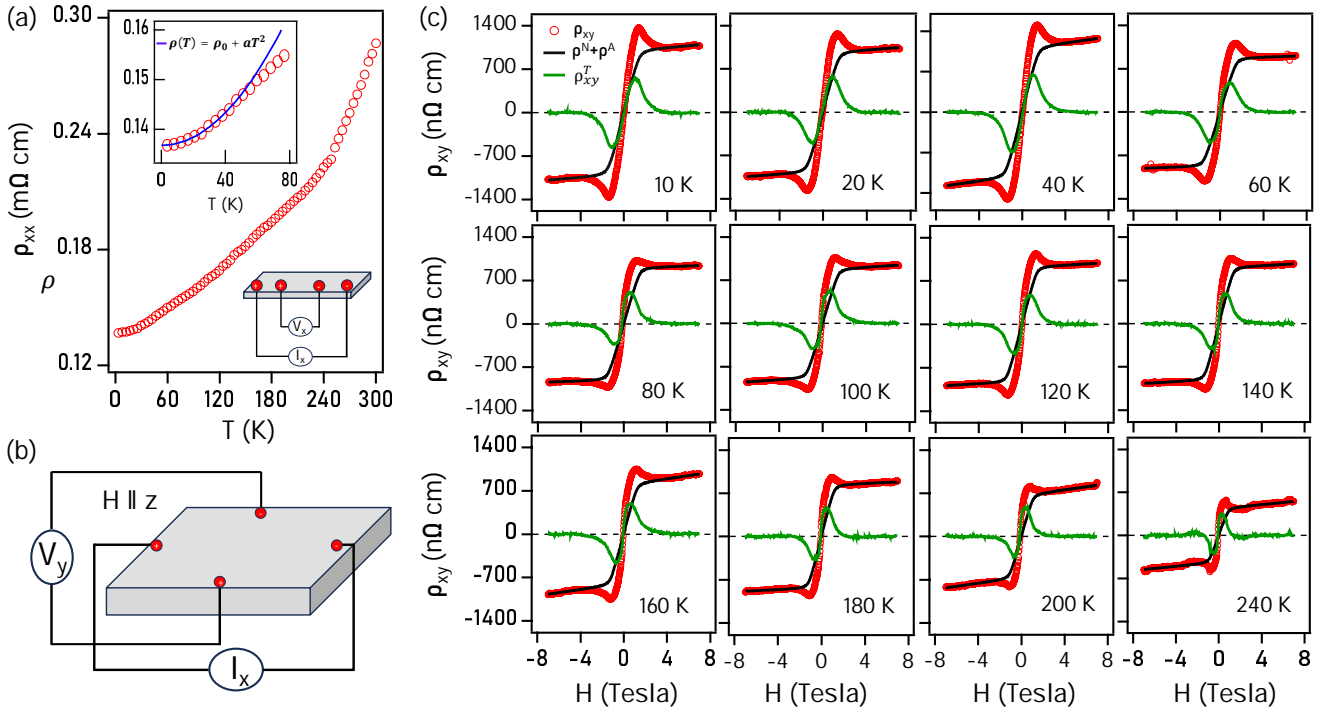


Figure 5: (a) Temperature-dependent longitudinal electrical resistivity ρ_{xx} . The top inset of (a) displays low-temperature resistivity fitted by $\rho(T) = \rho_0 + aT^2$ and the bottom inset of (a) shows a schematic of linear four-probe geometry. (b) Schematic diagram of the Hall measurement geometry. (c) Transverse resistivity ρ_{xy} (Hall resistivity), ρ_{xy} plotted as a function of the magnetic field measured at various temperatures. In (c), the red curves represent total Hall resistivity (raw data), the black curves are the fittings using the equation $\rho_N + \rho_A$, and the green curves represent the topological Hall resistivity (ρ_T). See the text for more details.

$$\theta_+ = (T - T_C)/(T_{r2} - T_C), T > T_C \quad (11)$$

Following the MCE scaling analysis, all the curves of $\frac{\Delta S_m}{\Delta S_m^{max}}$ plotted as a function of reduced temperature θ at various magnetic fields collapse into a single curve as shown in Fig. 4(d), confirming the second-order magnetic phase transition in Cr_{0.83}Te [59, 60, 90]. Moreover, it can be seen that the universal curve of MCE is independent of the applied magnetic field and temperature, as it is generally determined by the intrinsic magnetization of the system [87]. Further, the reference temperatures T_{r1} and T_{r2} linearly depend on $H^{1/\Delta}$ for $\Delta = \beta + \gamma$ as shown in Fig. 4(e). Fig. 4(f) displays the temperature dependence of p . The $p(T)$ curve follows universal behavior across T_C as it reaches the value 1 for $T < T_C$ [91]. On the other hand, well above T_C , p reaches the value of two due to the Curie-Weiss law [91]. At $T = T_C$, $p(T)$ has a minimum value of 0.7, in line with the universal law of $p(T)$ [59]. Overall, the temperature dependence of p perfectly follows the universal behavior of a second-order phase transition [87]. The rotational magnetic entropy changes (ΔS_m^R) can be calculated using the formula $\Delta S_m^R(T, H) = \Delta S_m(T, H_{ab}) - \Delta S_m(T, H_c)$. Fig. 4(g) depicts the temperature dependence of $-\Delta S_m^R(T, H)$. From Fig. 4(g), we can find a maximum of $-\Delta S_m^R(T, H)$ at around T_C when derived at a field interval of 0.2 T. The maxima of $-\Delta S_m^R(T, H)$ shifts to lower temperatures with increasing

field intervals, and for 2 T of field interval, no maxima is found down to 315 K. This behavior is generally found in systems with strong magnetic anisotropy [23].

3.3. Electrical and Magnetotransport Properties

Figure 5(a) displays temperature-dependent longitudinal resistivity ρ_{xx} of Cr_{0.83}Te single crystal, revealing the metallic nature throughout the measured temperature range [92]. A change in the resistivity curve is noticed at around 245 K, while the exact origin is not very clear to us, but we noticed a small cusp in the dM/dT (not shown) at around 245 K from the FC data measured with 0.02 T [see Fig. 2(a)]. The top inset of Fig. 5(a) elucidates the quadratic temperature dependence of ρ_{xx} , fitted by $\rho(T) = \rho_0 + aT^2$, indicating dominant electron-electron scattering at low temperatures. This observation is in agreement with the theoretical studies on weak itinerant ferromagnetic metals in which a T^2 dependence of ρ_{xx} was predicted at low temperatures [93]. The bottom inset of Fig. 5(a) depicts the linear four-probe geometry used for measuring the longitudinal resistivity. The transverse resistivity ρ_{xy} (Hall resistivity) as a function of the applied field (H) is shown in Fig. 5(c) measured at various sample temperatures. The Hall resistivity, ρ_{xy} , was measured with the current applied along the x -axis, the magnetic field applied along the z -axis, and the resulting Hall voltage was detected along the y -axis as demonstrated in Fig. 5(b). Thus, the red-colored curves shown in the panels of Fig. 5(c) exhibit the raw data of field-dependent Hall

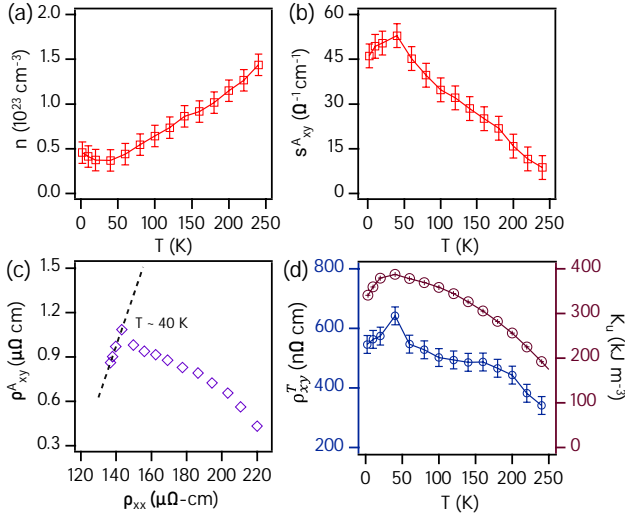


Figure 6: Temperature dependence of (a) derived calculated carrier density n . (b) Anomalous Hall conductivity σ_{xy}^A . (c) Plot of ρ_{xy}^A vs. ρ_{xx} with linear fitting up to 40 K. (d) Maximum value of topological Hall resistivity $\rho_{xy}^{T,max}$ (left axis) and magnetocrystalline anisotropy density, K_u (right axis), plotted as a function of temperature.

resistivity ρ_{xy} recorded at various sample temperatures, and the black-colored curves are the fittings to the total Hall resistivity using the formula [94],

$$\rho_{xy}(H) = \rho^N(H) + \rho^A(H) = \mu_0 R_0 H + \mu_0 R_s M \quad (12)$$

Here, ρ^N and ρ^A are the normal Hall and anomalous Hall contributions to the total Hall resistivity, respectively. R_0 is the normal Hall coefficient, R_s is the anomalous Hall coefficient, and M is the isothermal magnetization. The normal and anomalous Hall coefficients can be determined by a linear fit at the high field region following the relation $\frac{\rho_{xy}}{\mu_0 H} = R_0 + \frac{R_s M}{H}$, as shown in Fig. S1 of the supplemental information. However, as can be seen from the panels of Fig. 5(c), the fitting of ρ_{xy} with Eq. 12 is not perfect due to the topological Hall contribution. Thus, by including the topological Hall effect (THE) contribution, the total Hall resistivity can be expressed by $\rho_{xy}(H) = \mu_0 R_0 H + \mu_0 R_s M + \rho^T$ and the topological Hall resistivity (ρ^T) is extracted using the relation $\rho^T = \rho_{xy}(H) - (\mu_0 R_0 H + \mu_0 R_s M)$ [42, 95]. In Fig. 5(c), the green-colored curves represent the topological Hall resistivity.

Figure 6(a) depicts the charge-carrier density (n) plotted as a function of temperature, estimated from the normal Hall coefficient R_0 following the relation $n = 1/(R_0 q)$. Here q is the hole-carrier charge. The derived carrier concentration n decreases with increasing temperature up to 40 K. However, above 40 K, it increases monotonously with temperature. In Cr_xTe_y systems, the competition between the FM and AFM phases plays a vital role in the magnetotransport properties [41, 42, 44]. Similarly, in Fig. 2(f), the in-plane

$\Delta M(T)$ changes abruptly around $T \approx 40$ K, plausibly originating the non-monotonic changes of carrier concentration around 40 K. Next, the anomalous Hall conductivity (AHC), σ_{xy} , obtained using the relation $\sigma_{xy} = \frac{\rho_{xy}}{\rho_{xy}^2 + \rho_{xx}^2}$ is presented in Fig. 6(b). σ_{xy} increases with increasing temperature up to 40 K. Beyond 40 K, it monotonically decreases with increasing temperature. A maximum $\sigma_{xy} \approx 52 \Omega^{-1} \text{ cm}^{-1}$ is found at around 40 K. In general, the anomalous Hall conductivity can intrinsically arise from the electronic structure-originated non-zero Berry curvature [94, 96] or extrinsically due to magnetism-originated side-jump/skew-scattering mechanisms [94, 97].

To understand the nature of AHE in Cr_{0.83}Te we plotted ρ_{xy} vs. ρ_{xx} in Fig. 6(c). The Hall resistivity for an itinerant ferromagnetic metal is generally expressed by the formula $\rho_{xy} = \alpha \rho_{xx} + \beta \rho_{xx}^2$, where α and β represent the skew-scattering and side-jump coefficients, respectively [94, 98]. From Fig. 6(c), a linear dependence of ρ_{xy} on ρ_{xx} is evident up to 40 K, beyond which a deviation occurs with increasing temperature. This observation hints at the skew-scattering mechanism that originated anomalous Hall effect in Cr_{0.83}Te, consistent with the other Cr_xTe_y systems [42, 92, 99]. Furthermore, Fig. 6(d) depicts the maximum amplitude of topological Hall resistivity ($\rho_{xy}^{T,max}$) (left axis) plotted as a function of temperature. $\rho_{xy}^{T,max}$ increases with temperature and reaches a maximum value of approximately 620 n Ω -cm at around 40 K, consistent with $\Delta M(T)$ ($H \parallel xy$) of Fig. 2(f). The right axis of Fig. 6(d) displays the magnetocrystalline anisotropy energy constant, K_u , calculated using Eq. 3. It is worth mentioning here that the critical point of 40 K observed from ρ_{xy}^A , ρ_{xy}^T , and K_u (see Fig. 6) originates from a canted antiferromagnetic transition noticed at around 40 K (from $M(T)$ measured with 2 T, not shown), which is consistent with the other Cr_xTe_y based systems [64, 67].

Several theories have been proposed to elucidate the origin of the chiral spin texture that can manifest the topological Hall effect. These theories include the Dzyaloshinskii-Moriya interaction (DMI) in noncentrosymmetric systems under a strong spin-orbit coupling [95, 100–103], geometrically frustrated magnetic interactions [104], and non-coplanar spin structure stabilized by the magnetocrystalline anisotropy (MCA) [42, 50]. On the other hand, the intricate magnetism observed in Cr_xTe_y type systems results from a complex interplay of magnetic interactions, including direct, super-exchange, and double exchange mechanisms, noncollinear magnetism, and a mixed valence state of the Cr ions [41, 58, 105]. The derived critical exponents, which deviate from any single universality class (as discussed above), strongly suggest the presence of robust magnetocrystalline anisotropy (MCA) in Cr_{0.83}Te. Consequently, the large MCA can stabilize the requisite chiral spin structure [49, 106]. Thus, in the presence of chiral-spin structure, the itinerant electrons acquire real-space Berry curvature, leading to a non-zero scalar-spin chirality $\chi_{ijk} = S_i(S_j \times S_k) \neq 0$ to produce the topological Hall effect [102, 104]. The

analogy of chiral-spin structure stabilized by the large MCA is consistent with our experimental data shown in Fig. 6(d) (right-axis), where the temperature-dependent topological Hall resistivity (ρ_{xy}^T) replicates the temperature dependence of MCA energy density K_u , having the maximum ρ_{xy}^T at the maximum $K_u \approx 390 \text{ kJ/m}^3$ at 40 K.

4. Summary

We investigated the intricate magnetism, electrical, and magnetotransport properties in the hexagonal itinerant ferromagnet Cr_{0.83}Te. The magnetotransport study reveals a substantial topological Hall effect, originating from the non-coplanar spin structure in the presence of strong magnetic anisotropy and the skew-scattering-induced anomalous Hall effect. We observe a remarkable cooling efficacy of $-\Delta S_m^{\max} \approx 2.77 \text{ J kg}^{-1} \text{ K}^{-1}$ and RCP $\approx 88.29 \text{ J/kg}$ at an applied field of 5 Tesla. By utilizing the magneto-entropy scaling analysis, we extracted the critical exponents $\beta = 0.4739(4)$, $\gamma = 1.2812(3)$, and $\delta = 3.7037(5)$, which do not follow any single universality class, suggesting a complex magnetic interaction in Cr_{0.83}Te. Re-scaled $-\Delta S_m(T, H)$ curves fall into a single universal curve, confirming the second-order magnetic transition. The spin-fluctuation parameter, derived from the critical magnetization isotherms based on the SCR theory, confirms the itinerant ferromagnetic nature of Cr_{0.83}Te.

5. Acknowledgements

S.C. and S.G. acknowledge the University Grants Commission (UGC), India, for the PhD fellowship. Part of this work has been done using instruments from the Technical Research Centre (TRC) of the S. N. Bose National Centre for Basic Sciences, established under the TRC project of the Department of Science and Technology (DST), Govt. of India.

References

- [1] H. Liu, Y. Zhang, O. E. Glukhova, G. Zhang, L. Wang, J. Zhao, J. Gao, Interlayer Hopping Kinetics of Vacancies in CrI₃ Layers Leading to Monolayer/Bilayer Heterostructures, *Adv. Mater. Interfaces* 9 (2022) 2200626.
- [2] A. Soumyanarayanan, N. Reyren, A. Fert, C. Panagopoulos, Emergent phenomena induced by spin-orbit coupling at surfaces and interfaces, *Nature* 539 (2016) 509–517.
- [3] Y. Deng, Y. Yu, Y. Song, J. Zhang, N. Z. Wang, Z. Sun, Y. Yi, Y. Z. Wu, S. Wu, J. Zhu, et al., Gate-tunable room-temperature ferromagnetism in two-dimensional Fe₃GeTe₂, *Nature* 563 (2018) 94–99.
- [4] B. Wang, Y. Zhang, L. Ma, Q. Wu, Y. Guo, X. Zhang, J. Wang, MnX (X = P, As) monolayers: a new type of two-dimensional intrinsic room temperature ferromagnetic half-metallic material with large magnetic anisotropy, *Nanoscale* 11 (2019) 4204–4209.
- [5] A. K. Geim, I. V. Grigorieva, Van der Waals heterostructures, *Nature* 499 (2013) 419–425.
- [6] J. T. Heron, M. Trassin, K. Ashraf, M. Gajek, Q. He, S. Y. Yang, D. E. Nikonov, Y.-H. Chu, S. Salahuddin, R. Ramesh, Electric-Field-Induced Magnetization Reversal in a Ferromagnet-Multiferroic Heterostructure, *Phys. Rev. Lett.* 107 (2011) 217202.
- [7] Y. Khan, S. M. Obaidulla, M. R. Habib, A. Gayen, T. Liang, X. Wang, M. Xu, Recent breakthroughs in two-dimensional van der Waals magnetic materials and emerging applications, *Nano Today* 34 (2020) 100902.
- [8] M. Hossain, B. Qin, B. Li, X. Duan, Synthesis, characterization, properties and applications of two-dimensional magnetic materials, *Nano Today* 42 (2022) 101338.
- [9] C. Gong, L. Li, Z. Li, H. Ji, A. Stern, Y. Xia, T. Cao, W. Bao, C. Wang, Y. Wang, et al., Discovery of intrinsic ferromagnetism in two-dimensional van der Waals crystals, *Nature* 546 (2017) 265–269.
- [10] K. L. Seyler, D. Zhong, D. R. Klein, S. Gao, X. Zhang, B. Huang, E. Navarro-Moratalla, L. Yang, D. H. Cobden, M. A. McGuire, et al., Ligand-field helical luminescence in a 2D ferromagnetic insulator, *Nat. Phys.* 14 (2018) 277–281.
- [11] Z. Fei, B. Huang, P. Malinowski, W. Wang, T. Song, J. Sanchez, W. Yao, D. Xiao, X. Zhu, A. F. May, et al., Two-dimensional itinerant ferromagnetism in atomically thin Fe₃GeTe₂, *Nat. Mater.* 17 (2018) 778–782.
- [12] M. Gibertini, M. Koperski, A. F. Morpurgo, K. S. Novoselov, Magnetic 2D materials and heterostructures, *Nat. Nanotechnol.* 14 (2019) 408–419.
- [13] H. L. Zhuang, P. R. C. Kent, R. G. Hennig, Strong anisotropy and magnetostriction in the two-dimensional Stoner ferromagnet Fe₃GeTe₂, *Phys. Rev. B* 93 (2016) 134407.
- [14] Mermin, N. D. and Wagner, H., Absence of Ferromagnetism or Antiferromagnetism in One- or Two-Dimensional Isotropic Heisenberg Models, *Phys. Rev. Lett.* 17 (1966) 1133–1136.
- [15] B. Huang, G. Clark, E. Navarro-Moratalla, D. R. Klein, R. Cheng, K. L. Seyler, D. Zhong, E. Schmidgall, M. A. McGuire, D. H. Cobden, W. Yao, D. Xiao, P. Jarillo-Herrero, X. Xu, Layer-dependent ferromagnetism in a van der Waals crystal down to the monolayer limit, *Nature* 546 (2017) 270–273.
- [16] Y. Liu, C. Petrovic, Critical behavior of quasi-two-dimensional semiconducting ferromagnet Cr₂Ge₂Te₆, *Phys. Rev. B* 96 (2017) 054406.
- [17] T. J. Williams, A. A. Aczel, M. D. Lumsden, S. E. Nagler, M. B. Stone, J.-Q. Yan, D. Mandrus, Magnetic correlations in the quasi-two-dimensional semiconducting ferromagnet CrSiTe₃, *Phys. Rev. B* 92 (2015) 144404.
- [18] Q. Xie, Y. Liu, M. Wu, H. Lu, W. Wang, L. He, X. Wu, Two stage magnetization in van der Waals layered CrXTe₃ (X = Si, Ge) single crystals, *Mater. Lett.* 246 (2019) 60–62.
- [19] X. Feng, J. Li, J. Wu, Anisotropy of magnetocaloric effect in Fe₃GeTe₂, *Phys. B Condens. Matter* 625 (2022) 413478.
- [20] X. Sun, S. Zhao, A. Bachmatiuk, M. H. Rummeli, S. Gorantla, M. Zeng, L. Fu, 2D Intrinsic Ferromagnetic MnP Single Crystals, *Small* 16 (2020) 2001484.
- [21] L. M. Moreno-Ramírez, V. Franco, Reversibility of the Magnetocaloric Effect in the Bean-Rodbell Model, *Magnetochemistry* 7 (2021) 60.
- [22] V. Y. Verchenko, A. A. Tsirlin, A. V. Sobolev, I. A. Presniakov, A. V. Shevelkov, Ferromagnetic Order, Strong Magnetocrystalline Anisotropy, and Magnetocaloric Effect in the Layered Telluride Fe₃GeTe₂, *Inorg. Chem.* 54 (2015) 8598–8607.
- [23] Y. Liu, M. Abeykoon, E. Stavitski, K. Attenkofer, C. Petrovic, Magnetic anisotropy and entropy change in trigonal Cr₅Te₈, *Phys. Rev. B* 100 (2019) 245114.
- [24] Y. Liu, C. Petrovic, Anisotropic magnetic entropy change in Cr₂X₂Te₆ (X = Si and Ge), *Phys. Rev. Materials* 3 (2019) 014001.
- [25] Y. Zhu, X. Kong, T. D. Rhone, H. Guo, Systematic search for two-dimensional ferromagnetic materials, *Phys. Rev. Materials* 2 (2018) 081001.
- [26] T. Eto, M. Ishizuka, S. Endo, T. Kanomata, T. Kikegawa, Pressure-induced structural phase transition in a ferromagnet CrTe, *J. Alloys Compd.* 315 (2001) 16–21.

- [27] F. Wang, J. Du, F. Sun, R. F. Sabirianov, N. Al-Aqtash, D. Sengupta, H. Zeng, X. Xu, Ferromagnetic Cr_2Te_3 nanorods with ultrahigh coercivity, *Nanoscale* 10 (2018) 11028–11033.
- [28] B. Hessen, T. Siegrist, T. Palstra, S. Tanzler, M. Steigerwald, Hexakis (triethylphosphine) octatelluridohexachromium and a molecule-based synthesis of chromium telluride, Cr_3Te_4 , *Inorg. Chem.* 32 (1993) 5165–5169.
- [29] L.-Z. Zhang, A.-L. Zhang, X.-D. He, X.-W. Ben, Q.-L. Xiao, W.-L. Lu, F. Chen, Z. Feng, S. Cao, J. Zhang, J.-Y. Ge, Critical behavior and magnetocaloric effect of the quasi-two-dimensional room-temperature ferromagnet Cr_4Te_5 , *Phys. Rev. B* 101 (2020) 214413.
- [30] H. Liu, J. Fan, H. Zheng, J. Wang, C. Ma, H. Wang, L. Zhang, C. Wang, Y. Zhu, H. Yang, Magnetic properties and critical behavior of quasi-2D layered Cr_4Te_5 thin film, *Front. Phys.* 18 (2023) 13302.
- [31] W. Wang, J. Fan, H. Liu, H. Zheng, C. Ma, L. Zhang, Y. Sun, C. Wang, Y. Zhu, H. Yang, Fabrication and magnetic-electronic properties of van der Waals Cr_4Te_5 ferromagnetic films, *CrystEngComm* 24 (2022) 674–680.
- [32] Y. Wang, J. Yan, J. Li, S. Wang, M. Song, J. Song, Z. Li, K. Chen, Y. Qin, L. Ling, H. Du, L. Cao, X. Luo, Y. Xiong, Y. Sun, Magnetic anisotropy and topological Hall effect in the trigonal chromium tellurides Cr_5Te_8 , *Phys. Rev. B* 100 (2019) 024434.
- [33] X.-H. Luo, W.-J. Ren, Z.-D. Zhang, Magnetic properties and magnetocaloric effect of a trigonal Te -rich Cr_5Te_8 single crystal, *J. Magn. Magn. Mater.* 445 (2018) 37–43.
- [34] J. Dijkstra, H. Weitering, C. Van Bruggen, C. Haas, R. De Groot, Band-structure calculations, and magnetic and transport properties of ferromagnetic chromium tellurides (CrTe , Cr_3Te_4 , Cr_2Te_3), *J. Phys.: Condens. Matter* 1 (1989) 9141.
- [35] Z.-L. Huang, W. Bensch, D. Benea, H. Ebert, Anion substitution effects on structure and magnetism in the chromium chalcogenide Cr_5Te_8 —Part I: Cluster glass behavior in trigonal $\text{Cr}(1+x)\text{Q}_2$ with basic cell ($\text{Q}=\text{Te}$, Se ; $\text{Te}:\text{Se}=7:1$), *J. Solid State Chem.* 177 (2004) 3245–3253.
- [36] Z.-L. Huang, W. Bensch, S. Mankovsky, S. Polesya, H. Ebert, R. K. Kremer, Anion substitution effects on structure and magnetism of the chromium chalcogenide Cr_5Te_8 Part II: Cluster-glass and spin-glass behavior in trigonal $\text{Cr}(1+x)\text{Q}_2$ with basic cells and trigonal $\text{Cr}(5+x)\text{Q}_8$ with superstructures ($\text{Q}=\text{Te}$, Se ; $\text{Te}:\text{Se}=6:2$), *J. Solid State Chem.* 179 (2006) 2067–2078.
- [37] J. Wontcheu, W. Bensch, S. Mankovsky, S. Polesya, H. Ebert, R. K. Kremer, E. Brücher, Anion substitution effects on the structure and magnetism of the chromium chalcogenide Cr_5Te_8 —Part III: Structures and magnetism of the high-temperature modification $\text{Cr}(1+x)\text{Q}_2$ and the low-temperature modification $\text{Cr}(5+x)\text{Q}_8$ ($\text{Q}=\text{Te}$, Se ; $\text{Te}:\text{Se}=5:3$), *J. Solid State Chem.* 181 (2008) 1492–1505.
- [38] H. Ipsen, K. L. Komarek, K. O. Klepp, Transition metal-chalcogen systems viii: The CrTe phase diagram, *Journal of the Less Common Metals* 92 (1983) 265–282.
- [39] C. Zhang, C. Liu, J. Zhang, Y. Yuan, Y. Wen, Y. Li, D. Zheng, Q. Zhang, Z. Hou, G. Yin, et al., Room-Temperature Magnetic Skyrmions and Large Topological Hall Effect in Chromium Telluride Engineered by Self-Intercalation, *Adv. Mater.* 35 (2023) 2205967.
- [40] B. Li, X. Deng, W. Shu, X. Cheng, Q. Qian, Z. Wan, B. Zhao, X. Shen, R. Wu, S. Shi, et al., Air-stable ultrathin Cr_3Te_4 nanosheets with thickness-dependent magnetic skyrmions, *Mater. Today* 57 (2022) 66–74.
- [41] Y. Chen, Y. Zhu, R. Lin, W. Niu, R. Liu, W. Zhuang, X. Zhang, J. Liang, W. Sun, Z. Chen, et al., Observation of colossal topological Hall effect in noncoplanar ferromagnet Cr_5Te_6 thin films, *Adv. Funct. Mater.* (2023) 2302984.
- [42] S. Purwar, A. Low, A. Bose, A. Narayan, S. Thirupathiah, Investigation of the anomalous and topological Hall effects in layered monoclinic ferromagnet $\text{Cr}_{2.76}\text{Te}_4$, *Phys. Rev. Mater.* 7 (2023) 094204.
- [43] M. Huang, L. Gao, Y. Zhang, X. Lei, G. Hu, J. Xiang, H. Zeng, X. Fu, Z. Zhang, G. Chai, et al., Possible Topological Hall Effect above Room Temperature in Layered $\text{Cr}_{1.2}\text{Te}_2$ Ferromagnet, *Nano Lett.* 21 (2021) 4280–4286.
- [44] J. Liu, B. Ding, J. Liang, X. Li, Y. Yao, W. Wang, Magnetic Skyrmionic bubbles at room temperature and sign reversal of the topological Hall effect in a layered ferromagnet $\text{Cr}_{0.87}\text{Te}$, *ACS Nano* 16 (2022) 13911–13918.
- [45] Y. He, J. Kroder, J. Gayles, C. Fu, Y. Pan, W. Schnelle, C. Felser, G. H. Fecher, Large topological Hall effect in an easy-cone ferromagnet $\text{Cr}_{0.9}\text{B}_{0.1}\text{Te}$, *Appl. Phys. Lett.* 117 (2020) 052409.
- [46] Kaul, SN, Static critical phenomena in ferromagnets with quenched disorder, *J. Magn. Magn. Mater.* 53 (1985) 5–53.
- [47] A. Bedoya-Pinto, J.-R. Ji, A. K. Pandeya, P. Gargiani, M. Valdivares, P. Sessi, J. M. Taylor, F. Radu, K. Chang, S. S. Parkin, Intrinsic 2D-XY ferromagnetism in a van der Waals monolayer, *Science* 374 (2021) 616–620.
- [48] S. Lee, J. Park, Y. Choi, K. Raju, W.-T. Chen, R. Sankar, K.-Y. Choi, Chemical tuning of magnetic anisotropy and correlations in $\text{Ni}_{1-x}\text{Fe}_x\text{PS}_3$, *Phys. Rev. B* 104 (2021) 174412.
- [49] M. Preißinger, K. Karube, D. Ehlers, B. Szigeti, H.-A. Krug von Nidda, J. S. White, V. Ukleev, H. M. Rønnow, Y. Tokunaga, A. Kikkawa, Y. Tokura, Y. Taguchi, I. Kézsmárki, Vital role of magnetocrystalline anisotropy in cubic chiral skyrmion hosts, *npj Quantum Materials* 6 (2021) 65.
- [50] A. Low, S. Ghosh, S. Changdar, S. Routh, S. Purwar, S. Thirupathiah, Tuning of topological properties in the strongly correlated antiferromagnet Mn_3Sn via Fe doping, *Phys. Rev. B* 106 (2022) 144429.
- [51] Y. Liu, C. Petrovic, Critical behavior of the quasi-two-dimensional weak itinerant ferromagnet trigonal chromium telluride $\text{Cr}_{0.62}\text{Te}$, *Phys. Rev. B* 96 (2017) 134410.
- [52] H. Liu, H. Zheng, Y. Wang, C. Huang, C. Ma, Y. Zhu, H. Yang, L. Ling, L. Zhang, J. Fan, Long-Range Magnetic Exchange Coupling in Quasi-2D CrTe Ferromagnetic Thin Films, *Phys. Status Solidi RRL* 17 (2023) 2300209.
- [53] H. Zheng, C. Huang, F. Lin, J. Fan, H. Liu, L. Zhang, C. Ma, C. Wang, Y. Zhu, H. Yang, Two-dimensional van der Waals ferromagnetic thin film CrTe_2 with high Curie temperature and metallic conductivity, *Appl. Phys. Lett.* 122 (2023) 023103.
- [54] H. Wu, W. Zhang, L. Yang, J. Wang, J. Li, L. Li, Y. Gao, L. Zhang, J. Du, H. Shu, et al., Strong intrinsic room-temperature ferromagnetism in freestanding non-van der Waals ultrathin 2D crystals, *Nat. Commun.* 12 (2021) 5688.
- [55] R. Sbiaa, H. Meng, S. N. Piramanayagam, Materials with perpendicular magnetic anisotropy for magnetic random access memory, *Phys. Status Solidi RRL* 5 (2011) 413–419.
- [56] D. L. Cortie, G. L. Causer, K. C. Rule, H. Fritzsche, W. Kreuzpaintner, F. Klose, Two-Dimensional Magnets: Forgotten History and Recent Progress towards Spintronic Applications, *Adv. Funct. Mater.* 30 (2020) 1901414.
- [57] V. Krizakova, E. Grimaldi, K. Garello, G. Sala, S. Couet, G. S. Kar, P. Gambardella, Interplay of Voltage Control of Magnetic Anisotropy, Spin-Transfer Torque, and Heat in the Spin-Orbit-Torque Switching of Three-Terminal Magnetic Tunnel Junctions, *Phys. Rev. Appl.* 15 (2021) 054055.
- [58] L.-Z. Zhang, Q.-L. Xiao, F. Chen, Z. Feng, S. Cao, J. Zhang, J.-Y. Ge, Multiple magnetic phase transitions and critical behavior in single crystal Cr_5Te_6 , *J. Magn. Magn. Mater.* 546 (2022) 168770.
- [59] Oesterreicher, H and Parker, FT., Magnetic cooling near Curie temperatures above 300 K, *J. Appl. Phys.* 55 (1984) 4334–4338.
- [60] J. Y. Law, V. Franco, L. M. Moreno-Ramírez, A. Conde, D. Y. Karpenkov, I. Radulov, K. P. Skokov, O. Gutfleisch, A quantitative criterion for determining the order of magnetic phase transitions using the magnetocaloric effect, *Nat. Commun.* 9 (2018) 1–9.
- [61] T. Hashimoto, K. Hoya, M. Yamaguchi, I. Ichitsubo, Magnetic properties of single crystals $\text{Cr}_{2-\delta}\text{Te}_3$, *J. Phys. Soc. Jpn.* 31 (1971) 679–682.

- [62] Ido, Hideaki and Shirakawa, Kiwamu and Suzuki, Takanobu and Kaneko, Takejiro, Exchange striction of ferromagnetic compound CrTe , *J. Phys. Soc. Jpn.* 26 (1969) 663–665.
- [63] F. Meng, W. Liu, A. Rahman, J. Zhang, J. Fan, C. Ma, M. Ge, T. Yao, L. Pi, L. Zhang, Y. Zhang, Crossover of critical behavior and nontrivial magnetism in the chiral soliton lattice host $\text{Cr}_{1/3}\text{TaS}_2$, *Phys. Rev. B* 107 (2023) 144425.
- [64] C. Li, K. Liu, D. Jiang, C. Jin, T. Pei, T. Wen, B. Yue, Y. Wang, Diverse Thermal Expansion Behaviors in Ferromagnetic $\text{Cr}_{1-\delta}\text{Te}$ with NiAs-Type, Defective Structures, *Inorg. Chem.* 61 (2022) 14641–14647.
- [65] C. Chen, X. Chen, C. Wu, X. Wang, Y. Ping, X. Wei, X. Zhou, J. Lu, L. Zhu, J. Zhou, et al., Air-Stable 2D Cr_5Te_8 Nanosheets with Thickness-Tunable Ferromagnetism, *Adv. Mater.* 34 (2022) 2107512.
- [66] L.-Z. Zhang, X.-D. He, A.-L. Zhang, Q.-L. Xiao, W.-L. Lu, F. Chen, Z. Feng, S. Cao, J. Zhang, J.-Y. Ge, Tunable Curie temperature in layered ferromagnetic $\text{Cr}_{5+\delta}\text{Te}_8$ single crystals, *APL Mater.* 8 (2020) 031101.
- [67] Z.-L. Huang, W. Kockelmann, M. Telling, W. Bensch, A neutron diffraction study of structural and magnetic properties of monoclinic Cr_7Te_8 , *Solid State Sci.* 10 (2008) 1099–1105.
- [68] A. Roy, S. Guchhait, R. Dey, T. Pramanik, C.-C. Hsieh, A. Rai, S. K. Banerjee, Perpendicular magnetic anisotropy and spin glass-like behavior in molecular beam epitaxy grown chromium telluride thin films, *ACS Nano* 9 (2015) 3772–3779.
- [69] Y. Fujisawa, M. Pardo-Almanza, J. Garland, K. Yamagami, X. Zhu, X. Chen, K. Araki, T. Takeda, M. Kobayashi, Y. Takeda, C. H. Hsu, F. C. Chuang, R. Laskowski, K. H. Khoo, A. Soumyanarayanan, Y. Okada, Tailoring magnetism in self-intercalated $\text{Cr}_{1+\delta}\text{Te}_2$ epitaxial films, *Phys. Rev. Mater.* 4 (2020) 114001.
- [70] K. Shimada, T. Saitoh, H. Namatame, A. Fujimori, S. Ishida, S. Asano, M. Matoba, S. Anzai, Photoemission study of itinerant ferromagnet $\text{Cr}_{1-\delta}\text{Te}$, *Phys. Rev. B* 53 (1996) 7673–7683.
- [71] Takahashi, Yoshinori, On the origin of the Curie-Weiss law of the magnetic susceptibility in itinerant electron ferromagnetism, *J. Phys. Soc. Jpn.* 55 (1986) 3553–3573.
- [72] M. Imai, C. Michioka, H. Ueda, K. Yoshimura, Static and dynamical magnetic properties of the itinerant ferromagnet LaCo_2P_2 , *Phys. Rev. B* 91 (2015) 184414.
- [73] S. Mondal, N. Khan, S. M. Mishra, B. Satpati, P. Mandal, Critical behavior in the van der Waals itinerant ferromagnet Fe_4GeTe_2 , *Phys. Rev. B* 104 (2021) 094405.
- [74] H. Ohta, C. Michioka, A. Matsuo, K. Kindo, K. Yoshimura, Magnetic study of SmCoAsO showing a ferromagnetic-antiferromagnetic transition, *Phys. Rev. B* 82 (2010) 054421.
- [75] Y. Takahashi, Spin fluctuation theory of itinerant electron magnetism, volume 9, Springer, 2013. URL: <https://doi.org/10.1007/978-3-642-36666-6>. doi:10.1007/978-3-642-36666-6.
- [76] N. Richter, D. Weber, F. Martin, N. Singh, U. Schwingenschlöggl, B. V. Lotsch, M. Kläui, Temperature-dependent magnetic anisotropy in the layered magnetic semiconductors CrI_3 and CrBr_3 , *Phys. Rev. Materials* 2 (2018) 024004.
- [77] J. Seo, D. Y. Kim, E. S. An, K. Kim, G.-Y. Kim, S.-Y. Hwang, D. W. Kim, B. G. Jang, H. Kim, G. Eom, et al., Nearly room temperature ferromagnetism in a magnetic metal-rich van der Waals metal, *Sci. Adv.* 6 (2020) eaay8912.
- [78] N. León-Brito, E. D. Bauer, F. Ronning, J. D. Thompson, R. Movshovich, Magnetic microstructure and magnetic properties of uniaxial itinerant ferromagnet Fe_3GeTe_2 , *J. Appl. Phys.* 120 (2016) 083903.
- [79] C. Zener, Classical Theory of the Temperature Dependence of Magnetic Anisotropy Energy, *Phys. Rev.* 96 (1954) 1335–1337.
- [80] Carr Jr, WJ, Temperature dependence of ferromagnetic anisotropy, *Phys. Rev.* 109 (1958) 1971.
- [81] V. K. Pecharsky, K. A. Gschneidner Jr, Magnetocaloric effect and magnetic refrigeration, *J. Magn. Magn. Mater.* 200 (1999) 44–56.
- [82] Arrott, Anthony, Criterion for Ferromagnetism from Observations of Magnetic Isotherms, *Phys. Rev.* 108 (1957) 1394–1396.
- [83] Y. Liu, J. Li, J. Tao, Y. Zhu, C. Petrovic, Anisotropic magnetocaloric effect in $\text{Fe}_{3-x}\text{GeTe}_2$, *Sci. Rep.* 9 (2019) 13233.
- [84] Y. Liu, C. Petrovic, Anisotropic magnetocaloric effect in single crystals of CrI_3 , *Phys. Rev. B* 97 (2018) 174418.
- [85] X. Yu, X. Zhang, Q. Shi, S. Tian, H. Lei, K. Xu, H. Hosono, Large magnetocaloric effect in van der Waals crystal CrBr_3 , *Front. Phys-beijing.* 14 (2019) 43501.
- [86] K. Gschneidner Jr, V. Pecharsky, A. Pecharsky, C. Zimm, Recent developments in magnetic refrigeration, in: *Materials science forum*, volume 315, Trans Tech Publ, 1999, pp. 69–76. URL: <https://doi.org/10.4028/www.scientific.net/MSF.315-317.69>. doi:10.4028/www.scientific.net/MSF.315-317.69.
- [87] V. Franco, J. Blázquez, A. Conde, Field dependence of the magnetocaloric effect in materials with a second order phase transition: A master curve for the magnetic entropy change, *Appl. Phys. Lett.* 89 (2006) 222512.
- [88] Widom, B., Degree of the critical isotherm, *J. Chem. Phys.* 41 (1964) 1633–1634.
- [89] V. Franco, C. Conde, J. Blázquez, A. Conde, P. Švec, D. Janičkovič, L. Kiss, A constant magnetocaloric response in FeMoCuB amorphous alloys with different Fe/B ratios, *J. Appl. Phys.* 101 (2007) 093903.
- [90] V. Franco, J. Law, A. Conde, V. Brabander, D. Karpenkov, I. Radulov, K. Skokov, O. Gutfleisch, Predicting the tricritical point composition of a series of LaFeSi magnetocaloric alloys via universal scaling, *J. Phys. D: Appl. Phys.* 50 (2017) 414004.
- [91] V. Franco, R. Caballero-Flores, A. Conde, Q. Dong, H. Zhang, The influence of a minority magnetic phase on the field dependence of the magnetocaloric effect, *J. Magn. Magn. Mater.* 321 (2009) 1115–1120.
- [92] Y. Liu, C. Petrovic, Anomalous Hall effect in the trigonal Cr_5Te_8 single crystal, *Phys. Rev. B* 98 (2018) 195122.
- [93] K. Ueda, T. Moriya, Contribution of spin fluctuations to the electrical and thermal resistivities of weakly and nearly ferromagnetic metals, *J. Phys. Soc. Jpn.* 39 (1975) 605–615.
- [94] N. Nagaosa, J. Sinova, S. Onoda, A. H. MacDonald, N. P. Ong, Anomalous Hall effect, *Rev. Mod. Phys.* 82 (2010) 1539–1592.
- [95] N. Kanazawa, Y. Onose, T. Arima, D. Okuyama, K. Ohoyama, S. Wakimoto, K. Kakurai, S. Ishiwata, Y. Tokura, Large Topological Hall Effect in a Short-Period Helimagnet MnGe , *Phys. Rev. Lett.* 106 (2011) 156603.
- [96] C. Zeng, Y. Yao, Q. Niu, H. H. Weitering, Linear magnetization dependence of the intrinsic anomalous Hall effect, *Phys. Rev. Lett.* 96 (2006) 037204.
- [97] Smit, Jan, The spontaneous Hall effect in ferromagnetics II, *Physica* 24 (1958) 39–51.
- [98] L. Berger, Side-Jump Mechanism for the Hall Effect of Ferromagnets, *Phys. Rev. B* 2 (1970) 4559–4566.
- [99] Z. Z. Jiang, X. Luo, J. Yan, J. J. Gao, W. Wang, G. C. Zhao, Y. Sun, J. G. Si, W. J. Lu, P. Tong, X. B. Zhu, W. H. Song, Y. P. Sun, Magnetic anisotropy and anomalous Hall effect in monoclinic single crystal Cr_5Te_8 , *Phys. Rev. B* 102 (2020) 144433.
- [100] S. D. Yi, S. Onoda, N. Nagaosa, J. H. Han, Skyrmions and anomalous Hall effect in a Dzyaloshinskii-Moriya spiral magnet, *Phys. Rev. B* 80 (2009) 054416.
- [101] Y. Li, N. Kanazawa, X. Z. Yu, A. Tsukazaki, M. Kawasaki, M. Ichikawa, X. F. Jin, F. Kagawa, Y. Tokura, Robust Formation of Skyrmions and Topological Hall Effect Anomaly in Epitaxial Thin Films of MnSi , *Phys. Rev. Lett.* 110 (2013) 117202.
- [102] H. Wang, Y. Dai, G.-M. Chow, J. Chen, Topological hall transport: Materials, mechanisms and potential applications, *Prog. Mater. Sci.* 130 (2022) 100971.
- [103] Q. Shao, Y. Liu, G. Yu, S. K. Kim, X. Che, C. Tang, Q. L. He, Y. Tserkovnyak, J. Shi, K. L. Wang, Topological Hall effect at above room temperature in heterostructures composed of a magnetic insulator and a heavy metal, *Nature Electronics* 2 (2019) 182–186.

- [104] Y. Machida, S. Nakatsuji, Y. Maeno, T. Tayama, T. Sakakibara, S. Onoda, Unconventional Anomalous Hall Effect Enhanced by a Noncoplanar Spin Texture in the Frustrated Kondo Lattice $\text{Pr}_2\text{Ir}_2\text{O}_7$, *Phys. Rev. Lett.* 98 (2007) 057203.
- [105] X. Zhang, B. Wang, Y. Guo, Y. Zhang, Y. Chen, J. Wang, High Curie temperature and intrinsic ferromagnetic half-metallicity in two-dimensional Cr_3X_4 (X= S, Se, Te) nanosheets, *Nanoscale Horiz.* 4 (2019) 859–866.
- [106] W. Wang, M. W. Daniels, Z. Liao, Y. Zhao, J. Wang, G. Koster, G. Rijnders, C.-Z. Chang, D. Xiao, W. Wu, Spin chirality fluctuation in two-dimensional ferromagnets with perpendicular magnetic anisotropy, *Nat. Mater.* 18 (2019) 1054–1059.